Bistability and criticality in the stochastic Wilson-Cowan model

Hanieh Alvankar Golpayegan [1] and Antonio de Candia [2,3]

[1]*Dipartimento di Neuroscienze, Scienze Riproduttive e Odontostomatologiche, Università di Napoli Federico II, Via S. Pansini 5, 80131 Napoli, Italy*

[2]*Dipartimento di Fisica "E. Pancini", Università di Napoli Federico II, Complesso Universitario di Monte Sant'Angelo, via Cintia, 80126 Napoli, Italy*

[3]*INFN, Sezione di Napoli, Gruppo collegato di Salerno, 84084 Fisciano (SA), Italy*

(Received 13 July 2022; revised 29 November 2022; accepted 17 February 2023; published 15 March 2023)

We study a stochastic version of the Wilson-Cowan model of neural dynamics, where the response function of neurons grows faster than linearly above the threshold. The model shows a region of parameters where two attractive fixed points of the dynamics exist simultaneously. One fixed point is characterized by lower activity and scale-free critical behavior, while the second fixed point corresponds to a higher (supercritical) persistent activity, with small fluctuations around a mean value. When the number of neurons is not too large, the system can switch between these two different states with a probability depending on the parameters of the network. Along with alternation of states, the model displays a bimodal distribution of the avalanches of activity, with a power-law behavior corresponding to the critical state, and a bump of very large avalanches due to the high-activity supercritical state. The bistability is due to the presence of a first-order (discontinuous) transition in the phase diagram, and the observed critical behavior is connected with the line where the low-activity state becomes unstable (spinodal line).

DOI: 10.1103/PhysRevE.107.034404

I. INTRODUCTION

Criticality and bistability are two fundamental features of the dynamics of cortical neural networks. The former shows up in the scale-free distribution of bursts of activity, first discovered by Beggs and Plenz in organotypic cultures from coronal slices of rat cortex [1], and confirmed in many other systems since then, in vivo [2–8] and in vitro [9–13], suggesting that the cortex operates at the edge of the critical phase transition between an ordered and a disordered phase [14–17]. This type of dynamic is believed to optimize dynamic range [18], information transmission, and information capacity [19]. Scale-free avalanches were reproduced also in many computational models of neural activity [20–23], among which is a stochastic version of the Wilson-Cowan model [24]. Recently, it has been shown [25] that the scale-free activity in the last model is connected to the presence of a continuous second-order transition in the attractive fixed point of the dynamics, where the characteristic size and duration of the bursts of activity scale with the system size, and the critical exponents of the scale-free distributions coincide with those of the critical branching model, as observed experimentally.

In some conditions, the dynamics of neural networks is characterized by the presence of a bistable activity that manifests as a bimodal distribution of avalanches of activity. This is usually found with the addiction of picrotoxin, which reduces inhibition in the system, or under epileptic or hyperexcitable conditions [1,9,26,27]. The bimodal distribution of avalanches reveals that the system switches between two states of the network, one characterized by critical avalanches, distributed as a power law, and another by very large, supercritical, avalanches [28]. Notably, recent results in magnetoencephalography [29] show that bistable criticality is a functionally significant feature of healthy awake resting-state brain dynamics, and clinically informative as a putative pathophysiological mechanism in epilepsy.

Here we exploit the Wilson-Cowan model of neural dynamics to explore the possibility that such bistability is due to a superlinear behavior in the activation function of neurons, such that the activation probability of a neuron grows faster than linearly with the input received from synapses [30]. Such superlinearity produces for some values of the parameters the simultaneous presence of two attractive fixed points in the dynamics, and a first-order discontinuous transition in the network activity as a function of a network parameter, for example, the strength of the synapses. Fluctuations in the dynamics, when the number of neurons is not too large, can produce transitions between the two states in the region of bistability, with the lifetime of states growing with the number of neurons. Near the instability line of the low-activity state, one observes a power-law distribution of the avalanches of activity, together with the presence of intervals of high activity (the supercritical state) whose duration depends on the parameter that defines the nonlinearity in the activation function. Differently from what was found in Ref. [25], the cutoff of the avalanche distribution is limited by the lifetime of the low-activity state, because very long avalanches switch with high probability to the high-activity state, characterized by an exponential distribution of the sizes. Note that the model we consider here is characterized by all-to-all connectivity between neurons, and therefore is suitable to describe the behavior of a single highly connected region of the brain. Therefore, beyond some system size, the behavior of the model might not be biologically relevant.

II. THE MODEL

We study a stochastic version of the Wilson-Cowan model of neural network [24,25,31], with N_E excitatory and N_I inhibitory neurons. The deactivation rate is α for all the neurons, while the activation rate is given by the activation function $f(s_i)$, where $s_i = \sum_j w_{ij}a_j + h_i$ is the synaptic input of the ith neuron, w_{ij} is the synaptic strength between neurons j and i, and $a_j = 0, 1$ if the neuron is active or quiescent. The external "fields" h_i represent the input to the ith neuron coming from neurons outside the considered network (for example, sensory neurons), and in principle may be a function of the neuron and of the time. Following the original formulation of the model, we set $h_i = h$ for all the neurons and constant in time. Moreover, we consider connections that depend only on the kind of presynaptic neuron, $w_{ij} = \frac{w_E}{N_E}$ if j is excitatory and $w_{ij} = -\frac{w_I}{N_I}$ if j is inhibitory. Therefore, the network is fully connected and the input $s_i \equiv s$ is equal for all the neurons. We emphasize here that in this case the only dynamical variables that have a role in the evolution of the system are the fractions of active excitatory and inhibitory neurons, so that the description in terms of individual neurons is strictly equivalent to the description in terms of populations.

Defining k and l respectively as the number of active excitatory and inhibitory neurons, with $0 \leqslant k \leqslant N_E$, $0 \leqslant l \leqslant N_I$, in the Gaussian noise approximation [24,32] one obtains the evolution equations

$$\frac{dk}{dt} = -\alpha k + (N_E - k)f(s) + \sqrt{\alpha k + (N_E - k)f(s)}\,\eta_E(t), \quad (1a)$$

$$\frac{dl}{dt} = -\alpha l + (N_I - l)f(s) + \sqrt{\alpha l + (N_I - l)f(s)}\,\eta_I(t), \quad (1b)$$

where $\eta_E(t)$ and $\eta_I(t)$ are white noises, with $\langle \eta_i(t)\rangle = 0$, $\langle \eta_i(t)\eta_j(t')\rangle = \delta_{ij}\delta(t - t')$, and $s = \frac{w_E}{N_E}k - \frac{w_I}{N_I}l + h$. Deterministic terms in Eqs. (1) are proportional to the numbers of neurons N_E and N_I, while the stochastic terms are proportional to $N_E^{1/2}$ and $N_I^{1/2}$. The fixed points of the dynamics correspond to the vanishing of the deterministic terms. Defining the total activity $\Sigma = \frac{1}{2}(\frac{k}{N_E} + \frac{l}{N_I})$, and the imbalance $\Delta = \frac{1}{2}(\frac{k}{N_E} - \frac{l}{N_I})$, the input is given by $s = w_0\Sigma + (w_E + w_I)\Delta + h$, where $w_0 = w_E - w_I$. The fixed points correspond to $\Delta = 0$ and $\Sigma = \Sigma_0$ satisfying the equation

$$\alpha\Sigma_0 = (1 - \Sigma_0)f(s_0), \quad (2)$$

where $s_0 = w_0\Sigma_0 + h$. To check if the fixed point is attractive or repulsive, one has to define $\Sigma = \Sigma_0 + N^{-1/2}\xi_\Sigma$, $\Delta = N^{-1/2}\xi_\Delta$, make a system size expansion of Eqs. (1) in powers of N, and consider only the leading terms, obtaining [24,25,31,32]

$$\frac{d}{dt}\begin{pmatrix}\xi_\Sigma \\ \xi_\Delta\end{pmatrix} = \begin{pmatrix}-1/\tau_1 & w_{\rm ff} \\ 0 & -1/\tau_2\end{pmatrix}\begin{pmatrix}\xi_\Sigma \\ \xi_\Delta\end{pmatrix} + \sqrt{\alpha\Sigma_0}\begin{pmatrix}\eta_\Sigma(t) \\ \eta_\Delta(t)\end{pmatrix}, \quad (3)$$

where $\tau_1^{-1} = \alpha + f(s_0) - (1 - \Sigma_0)w_0 f'(s_0)$, $\tau_2^{-1} = \alpha + f(s_0)$, $w_{\rm ff} = (1 - \Sigma_0)(w_E + w_I)f'(s_0)$, and $s_0 = w_0\Sigma_0 + h$. While τ_2 is always larger than zero, the sign of τ_1 determines if the fixed point is attractive ($\tau_1 > 0$), repulsive ($\tau_1 < 0$), or marginal ($\tau_1 = 0$). Note that, because connections depend only on the presynaptic neuron, the eigenvalues of the coupling matrix are always real, so that the system cannot display (at least in the linear regime) an oscillatory activity.

We consider here the activation function

$$f(s) = \begin{cases}\beta\tanh(s + \gamma s^2) & \text{if } s > 0 \\ 0 & \text{if } s \leqslant 0.\end{cases} \quad (4)$$

The case $\gamma = 0$ has been largely studied [24,25,31]. In particular in Ref. [25] it was shown that the model undergoes a continuous transition for $w_0 = w_c$, where $w_c = \beta^{-1}\alpha$. Indeed for $w_0 < w_c$, in the limit $h \to 0$, the fixed point is always given by $\Sigma = 0$, while for $w_0 > w_c$ such a fixed point becomes repulsive, and another attractive fixed point with $\Sigma > 0$ appears. Here we consider the case of a nonzero value of γ, that accounts for superlinear effects in the activation function [30].

In Fig. 1(a), we show the function $f(s)$ for different values of γ. The effect of a nonzero value of γ is that of producing the possibility of the simultaneous presence of more than one attractive fixed point in the dynamics [see Fig. 1(b)]. For a fixed value of w_0, above some critical value of γ a solution with $\Sigma > 0$ appears discontinuously, as shown in Fig. 1(c).

This kind of bistability is a feature of any activation function $f(s)$ that is convex in some interval of the input, as for example the sigmoidal $f(s) \propto (1 + e^{-s})^{-1}$. The function that we have considered here, however, combines this feature with the presence of a threshold, below which the activation function is zero. This means that the low-activity fixed point corresponds to a value of the activity that vanishes in the limit of external input $h \to 0$, so that the dynamics of the network is characterized by avalanches with a scale-free distribution, and a cutoff that scales with the number of neurons [25]. We expect, therefore, that for $\gamma > 0$ the network shows a coexistence between scale-free behavior alternating with intervals of (supercritical) high activity.

In the following, we will often express the activity of the network in terms of $R(t)$, the instantaneous firing rate per neuron. This is a simple function of Σ and Δ, namely, $R = (1 - \Sigma)f(s)$.

Numerical simulation methods

Unless otherwise stated, we set $\alpha = \beta = 0.1$ ms^{-1}, $h = 10^{-6}$, and $w_E + w_I = 13.8$, and study the behavior of the model for different numbers of neurons $N = N_E = N_I$, values of $w_0 = w_E - w_I$, and γ. We consider here the case $N_E = N_I$ as in the original formulation of the model (see, for example, Ref. [24]), although this is not realistic for typical biological neuronal systems. However, the overall behavior of the model depends mainly on the total input of neurons. Taking a different fraction of inhibitory and excitatory neurons, and compensating accordingly the relative strength of the connections, does not change in a critical way the outcome of the model. In particular the fixed-point equations do not change.

The network dynamics can be simulated in two ways, which are equivalent as soon as the number of neurons is not too small (with the exception of escape rates and probability of rare events; see Ref. [33]). The first is to simulate directly individual neurons, that is, to simulate the master equation of the system. This can be done by means of the event-driven Gillespie algorithm [34]. The steps of the algorithm are the

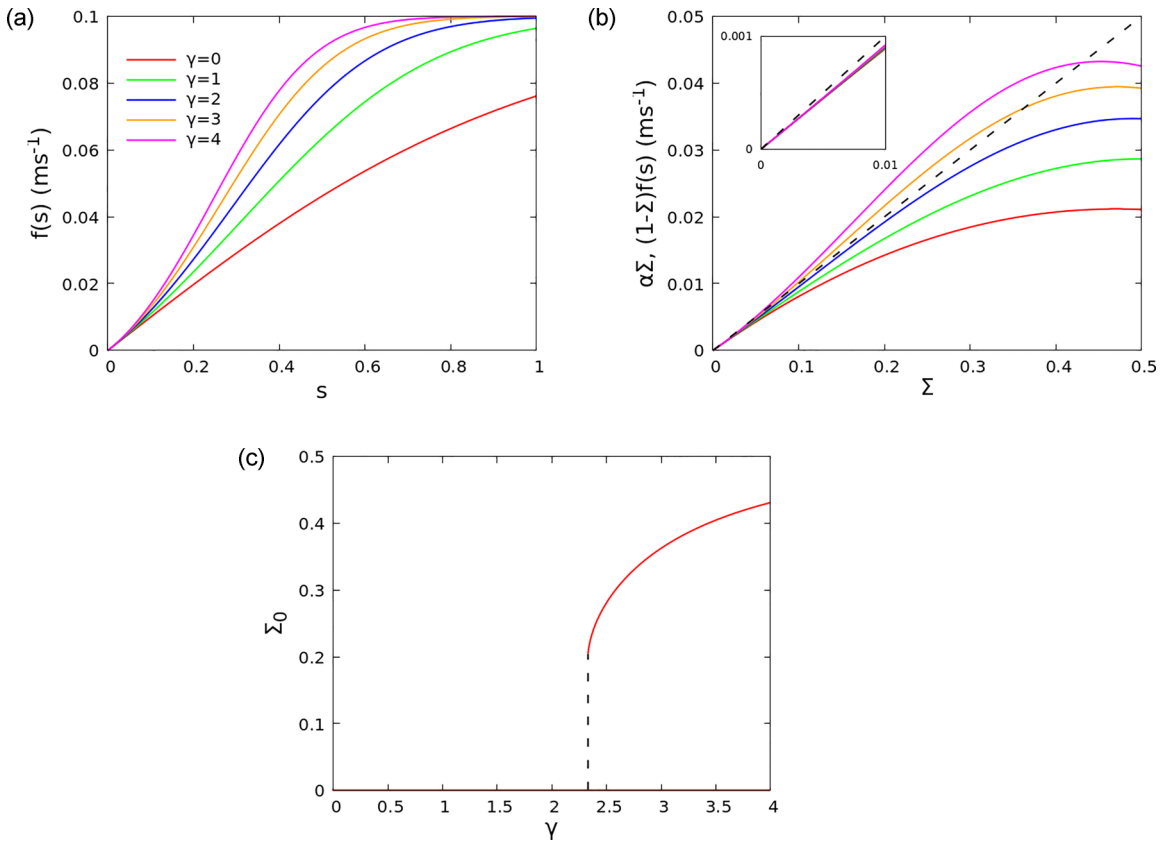

FIG. 1. (a) Activation functions $f(s)$ for $\gamma = 0, 1, 2, 3, 4$ (from bottom to top). (b) Plot of the two terms of Eq. (2), $\alpha\Sigma$ (dashed line) and $(1-\Sigma)f(s)$ (solid curves), where $s = w_0\Sigma + h$, for $\alpha = \beta = 0.1$ ms^{-1}, $w_0 = 0.9$, $h = 0$, and $\gamma = 0, 1, 2, 3, 4$ (from bottom to top). Attractive fixed points correspond to the crossing points where the solid curve has a lower derivative than the dashed line. For $\gamma < 2.33$ there is only one attractive fixed point at $\Sigma = 0$, while for $\gamma \geqslant 2.33$ another fixed point appears (discontinuously) at higher values of Σ. Inset: Zoom of the crossing of the curves at $\Sigma = 0$. (c) Values of Σ at the attractive fixed points, for $w_0 = 0.9$, $h = 0$, and $0 < \gamma < 4$. At $\gamma = 2.33$ a fixed point with $\Sigma > 0$ appears discontinuously.

following: (1) for each neuron i compute the transition rate r_i: $r_i = \alpha$ if neuron i is active, or $r_i = f(s_i)$ if it is quiescent; (2) compute the sum over all neurons $r = \sum_i r_i$; (3) draw a time interval dt from an exponential distribution with rate r; (4) choose the ith neuron with probability r_i/r and change its state; and (5) update the time to $t + dt$.

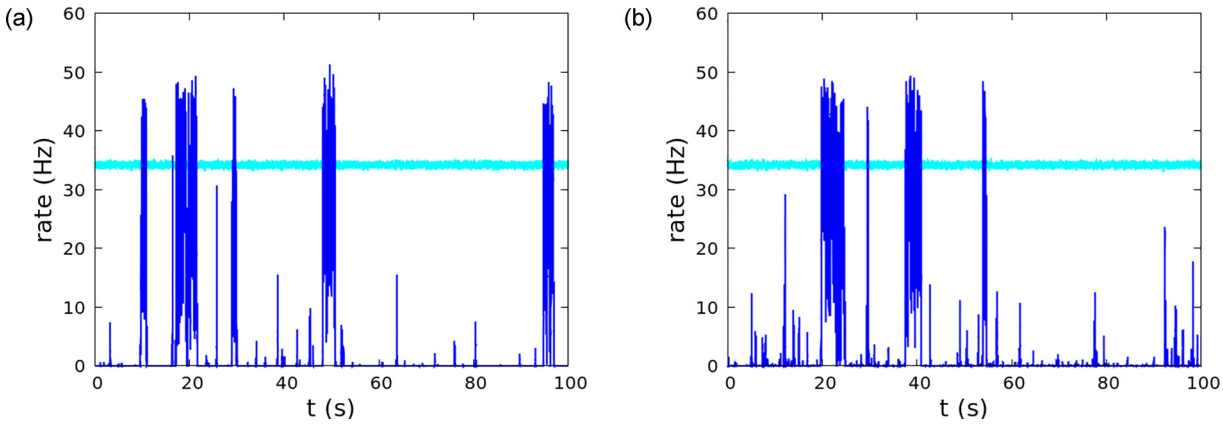

FIG. 2. Comparison between the dynamics of the network simulated by (a) the continuous-time Markov process and (b) the Langevin equations (1), for $\gamma = 2$, $w_0 = 1$, $N = 10^4$ (dark blue), and $N = 10^7$ (light cyan). In (a) the state of individual neurons is simulated using the event-driven Gillespie algorithm, while in (b) one uses the Gaussian noise approximation to simulate directly the variables k and l, representing the number of active excitatory and inhibitory neurons. While for $N = 10^4$ fluctuations are larger and the system switches frequently between different attractive fixed points, for $N = 10^7$ fluctuations are small and the switching is very unlikely (no switching is observed in the time window of the figure).

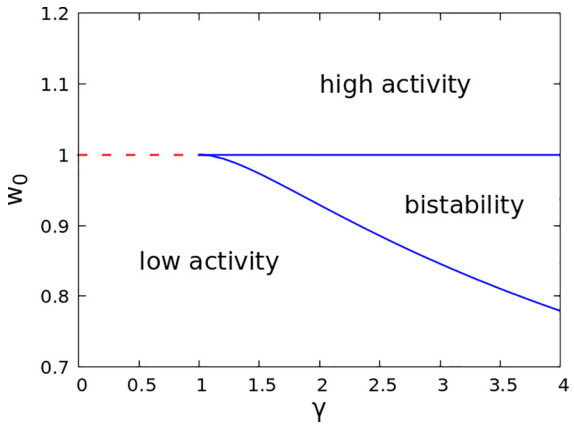

FIG. 3. Mean field phase diagram for $h \to 0$ and $\alpha = \beta$. The red dashed line is the continuous transition between the phase of low activity where $\Sigma_0 = 0$, and the phase of high activity where $\Sigma_0 > 0$. The lower blue solid line corresponds to the points where a solution $\Sigma_0 > 0$ appears discontinuously, and the upper blue solid line to the points where the solution $\Sigma_0 = 0$ becomes unstable. Between the blue solid lines there are two attractive fixed points of the network dynamics.

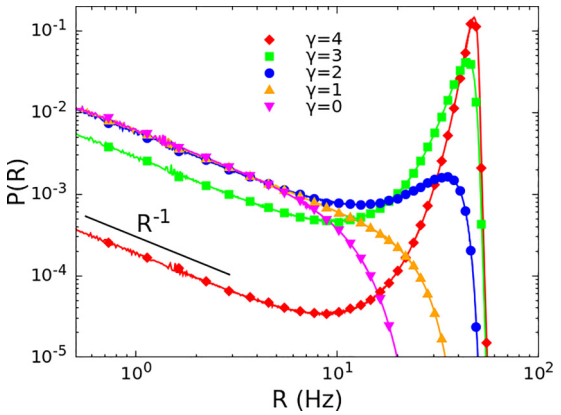

FIG. 4. Probability distribution of the firing rate R for $N_E = N_I = 10^4$, on the critical line $w_0 = 1$ and different values of γ.

The second way to simulate the system is to integrate directly the Langevin equations (1). As said before, when the system is fully connected as in the present case, the only dynamical variables are population variables, namely, the fractions of activated excitatory and inhibitory neurons, k/N_E and l/N_I. We can therefore directly compute the mean variations of k and l in a given interval of time, with a random Gaussian term that takes into account the expected fluctuations in the variations. The two approaches coincide when the number of neurons is not too small, with some exception as said above. In Fig. 2 we show a comparison between Gillespie algorithm [Fig. 2(a)] and Langevin equations [Fig. 2(b)] for $w_0 = 1$, $\gamma = 2$, $N = 10^4$ (blue), and $N = 10^7$ (cyan). In both cases the two approaches give rise to the same dynamics. For $N = 10^4$ even the switching time (that could be different in the two approaches) is similar. Of course the agreement holds in a "statistical" sense, because random noises are different in the two cases, but it can be verified quantitatively looking at averages and correlation functions (see Ref. [25]).

Note that for a very large number of neurons, namely, for $N \simeq 10^7$ with this set of parameters (cyan curve), the system fluctuates very near to an attractive fixed point. Even if more than one fixed point exists, fluctuations are too small to make the system switch to another one during the observation time. In this case the dynamics can be well described also by the linearized form (3) of the Langevin equations. In the following, unless otherwise stated, the system is simulated using the full master equation and Gillespie algorithm.

III. RESULTS

In Fig. 3 we show the mean field phase diagram of the model for small values of the external input h. With "mean field" behavior we mean that we only look at attractive fixed points of the dynamics, that is, solutions Σ_0 of Eq. (2) that correspond to negative eigenvalues of the matrix in Eq. (3). We call a fixed point such that the value of Σ_0 analytically goes to zero when $h \to 0$ a "low-activity fixed point," and a fixed point that goes to a finite value when $h \to 0$ a "high-activity fixed point." In the first case, for any number of neurons, there will be a value of the external input h so small that Σ_0 is equal to or smaller than the fluctuations of Σ, so that the activity frequently hits the value $\Sigma = 0$, and the dynamics of the network will be characterized by isolated bursts (avalanches) initiated by the small value of the input. In the second case, there will be a minimum value of N such that the network of neurons is able to sustain a continuous firing even when the external input goes to zero, so that the dynamics will be characterized by a self-sustained collective activity.

For $\gamma \leqslant \gamma_c$, where $\gamma_c = \alpha^{-1}\beta$, the behavior of the model does not change with respect to the case $\gamma = 0$. There is always one attractive fixed point, and a continuous transition at $w_0 = w_c$, with $w_c = \beta^{-1}\alpha$. For $w_0 \leqslant w_c$ the fixed point is a low-activity one, so that Σ_0 goes to zero when $h \to 0$, while for $w_0 > w_c$ it is a high-activity one, and remains finite when $h \to 0$. The line $w_0 = w_c$, $\gamma \leqslant \gamma_c$ (red line in Fig. 3) therefore can be seen as a line of second-order (continuous) phase transitions between a region of low activity and a region of high activity. On the other hand, when $\gamma > \gamma_c$, there exists a region $w_s(\gamma) < w_0 < w_c$ (the region between the blue lines in Fig. 3) where two attractive fixed points simultaneously exist. At the lower line $w_0 = w_s(\gamma)$, a high-activity fixed point appears discontinuously and coexists with the low-activity one. The latter in turn becomes unstable on the upper line $w_0 = w_c$.

When the network behavior is characterized by the low-activity fixed point, and therefore by isolated avalanches of activity, we expect a power-law distribution of avalanche sizes and durations, with a cutoff that depends on the distance from the critical value $w_0 = w_c$, that corresponds to the point where the low-activity fixed point becomes unstable [25]. This should hold both in the case of a second-order transition, as on the red line of Fig. 3, and in the case of a first-order transition on the "spinodal line" $w_0 = w_c$, as on the upper blue line of Fig. 3. When the network dynamics, on the other hand, is characterized by the high-activity fixed point, the activity fluctuates around its mean value, hitting zero only if a

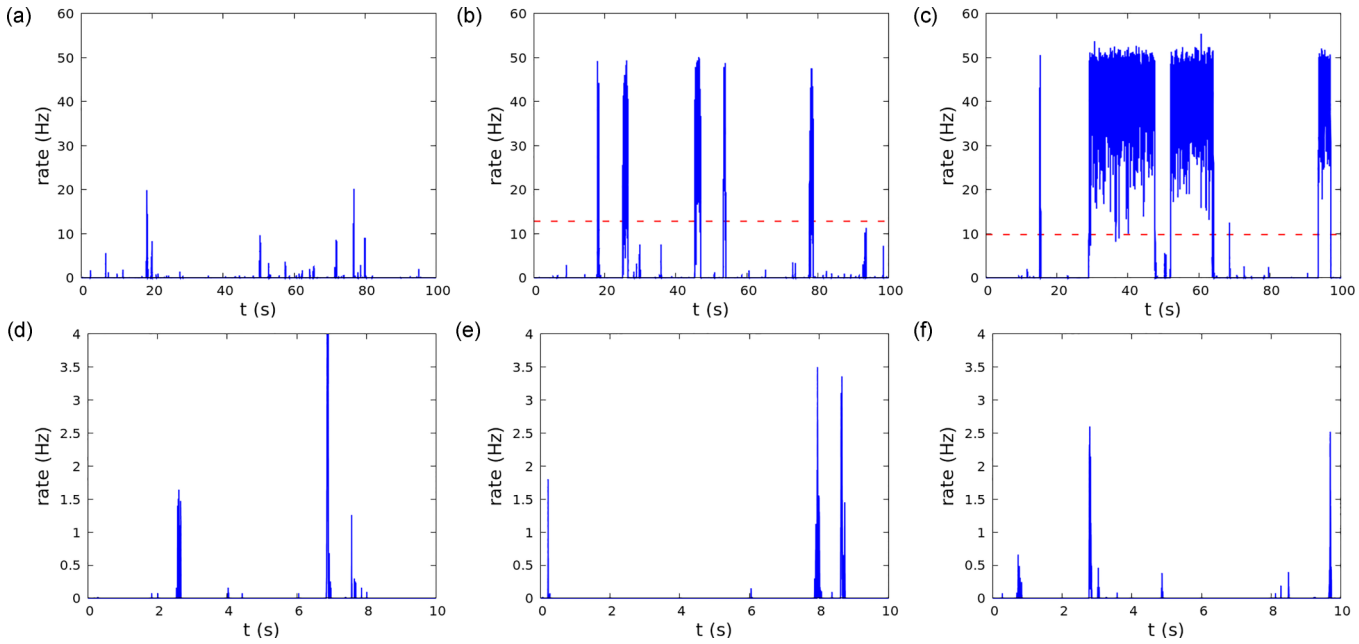

FIG. 5. Firing rate $R(t)$ as a function of time for $N_E = N_I = 10^4$, on the critical line $w_0 = 1$ and (from left to right) $\gamma = 1, 2, 3$. The red dashed line marks the value of the minimum in probability distribution of R (see Fig. 4). Lower row: Firing rate $R(t)$ with an enlarged scale to put in evidence the short bursts of activity that characterize the critical low-activity state.

large fluctuation occurs, which becomes less and less probable when the number of neurons grows.

In the bistable region, where two attractive fixed points exist, and for a finite number of neurons, the network activity can switch from the low-activity state to the high-activity one, therefore displaying an alternation of states.

We first study the probability distribution of the instantaneous firing rate $R(t)$, in a network simulated by the Gillespie algorithm. In Fig. 4 we show the probability distribution for $N_E = N_I = 10^4$, on the critical line, for different values of the parameter γ. While the peak at $R = 0$ Hz (low-activity critical state) is always present, for $\gamma > 1$ a peak at values of R around 40 Hz develops, corresponding to the high-activity (high-activity Poissonian state) fixed point.

The bimodal distribution of the network activity reflects itself in the bistable behavior of the network dynamics as a function of time. In this case one can observe transitions between the states of low and high activity of the network. In Fig. 5 we show the firing rate $R(t)$ of the network as a function of time. While at low values of γ the system remains in the low-activity state, where the activity is characterized by short bursts (avalanches) above zero, initiated by the external input h, for higher values of γ the system makes frequent switches to a state where the activity fluctuates around a constant value, and the network dynamics is self-sustained. The red dashed line marks the value R^* of the firing rate corresponding to the minimum in the probability distribution function (see Fig. 4). In the lower row of Fig. 5 we show the firing rate with an enlarged scale, to put in evidence that the short bursts of activity that characterize the critical low-activity state do not change notably when the parameter γ is increased.

On the other hand, the average time that the system spends in the two states changes markedly with γ. For the values of γ where the probability distribution of the firing rate R is bimodal and has a minimum, we define the value of R at the minimum as the threshold that discriminates between the two states. We then partition the time of the simulation in intervals where the system is continuously below or above the threshold, and compute the probability distribution of the durations of the intervals, shown in Fig. 6 for $N = 10^4, 2 \times 10^4$ and different values of γ on the critical line $w_0 = 1$. Both the distribution of the duration of low-activity and high-activity states can be well fitted by exponential functions (not shown), showing that the process of switching between the two states is Poissonian. This is what one may expect, considering that, inside the basin of attraction of a fixed point, dynamical variables decorrelate on a time scale much shorter than the time needed to escape from the basin due to a fluctuation of the noise. The average time of the states is shown in Fig. 7(a). By increasing the parameter γ for a fixed number of neurons, N, the average lifetime of the high-activity state, which corresponds to an attractive fixed point, increases quickly. On the other hand, the lifetime of the low-activity fixed point, which is marginal on the critical line $w_0 = 1$, decreases moderately. It is interesting to investigate how the lifetimes of the states depend on the number of neurons of the network. In Figs. 7(b) and 7(c) we plot the lifetimes as a function of N for two different points of phase space. In Fig. 7(b) for a point on the critical line, $\gamma = 3$, $w_0 = 1$. The lifetime of the state corresponding to the attractive fixed point increases exponentially with the number of neurons, while that of the critical low-activity state, whose fixed point is marginal, slowly decreases. In Fig. 7(c) we show instead the case of a point well inside the bistability region, $\gamma = 4$, $w_0 = 0.84$. In this case both fixed points are attractive, and the lifetimes of the states increase with the number of neurons both for the low-activity and for the high-activity state. Note that the exponential dependence of the lifetimes of attractive fixed points can be also derived

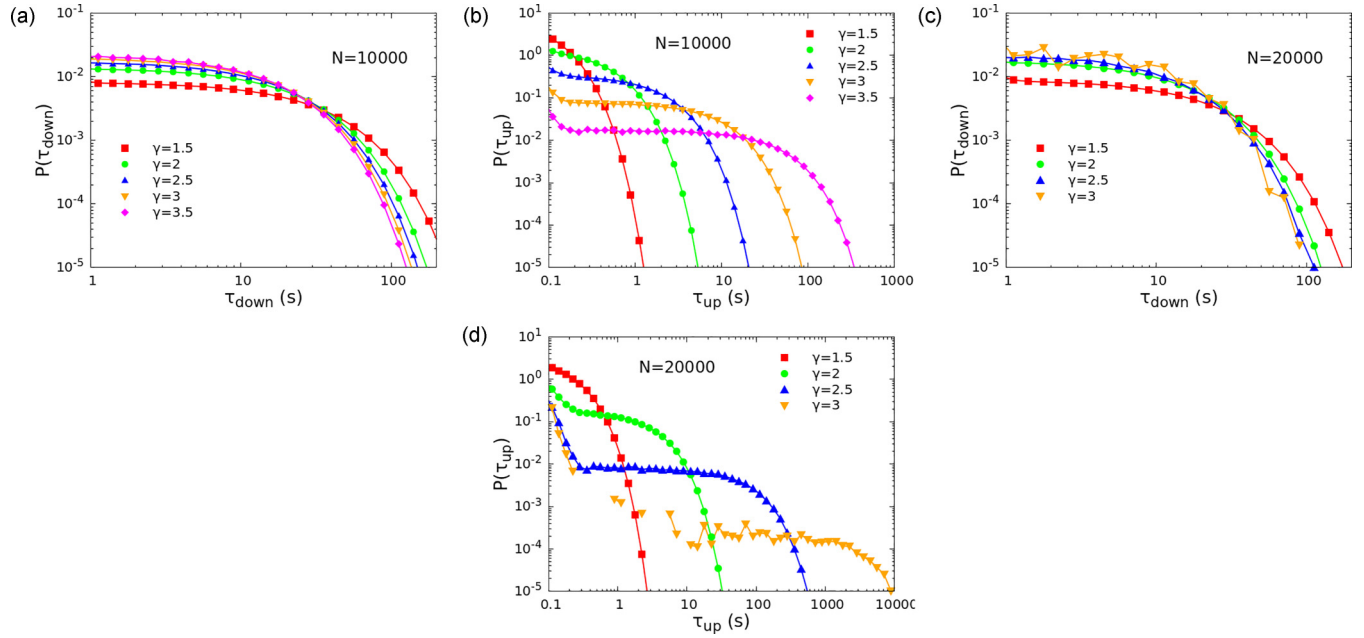

FIG. 6. Probability distribution of the lifetime of [(a), (c)] low-activity and [(b), (d)] high-activity states, for $N = 10^4$, 2×10^4, $w_0 = 1$, and different values of γ.

analytically using a Wentzel-Kramers-Brillouin (WKB) approximation [33]; however, this is quite burdening in the case of two populations, as in the present case.

A characteristic feature of systems displaying a first-order transition is that the state of the system depends on the past history. This can be put in evidence by simulating a hysteresis loop, in which the parameter w_0, measuring the difference between excitatory and inhibitory synapses, changes continuously from a low to a high value, and then back to the starting point. We simulate a system of $N = 10^5$ neurons, starting from $w_0 = 0.7$ and increasing the value of w_0 continuously to the value $w_0 = 1.1$ in 50 s, then decreasing it back to the initial value in another 50 s. In Fig. 8 we show the results for $\gamma = 0$ [Fig. 8(a)] and $\gamma = 4$ [Fig. 8(b)]. The red (blue) line shows the firing rate per neuron when w_0 is increased (decreased). When $\gamma = 0$ the system crosses a continuous (second-order) transition at $w_0 = 1$, so that only one attractive fixed point exists for any value of w_0, and the activity of the system does not depend on the past history. On the other hand, for $\gamma = 4$, the crossing of a first-order (discontinuous) transition reflects on the history-dependent behavior of the network activity.

Avalanche distributions and shapes

When $w_0 = 1$ and the external input h tends to zero, the low-activity fixed point is marginal, which means that one of the eigenvalues of the coupling matrix in Eq. (3) vanishes. This holds both on the second-order transition line ($w_0 = 1$, $\gamma < 1$) and on the higher spinodal ($w_0 = 1$, $\gamma > 1$) of the first-order transition line. In this case, the correlation time τ_1 and the fluctuations of the activity diverge in the linear approximation, which holds when the number of neurons $N \to \infty$, so that we expect that the system is characterized by a scale-free behavior with a cutoff that diverges with the number of neurons. This behavior should reflect on the distribution of the avalanches. Note, however, that, on the spinodal where the low-activity state has a finite lifetime, we do not expect a diverging cutoff of the first power-law regime, because very large avalanches will switch with high probability to the high-activity state, where the distribution of

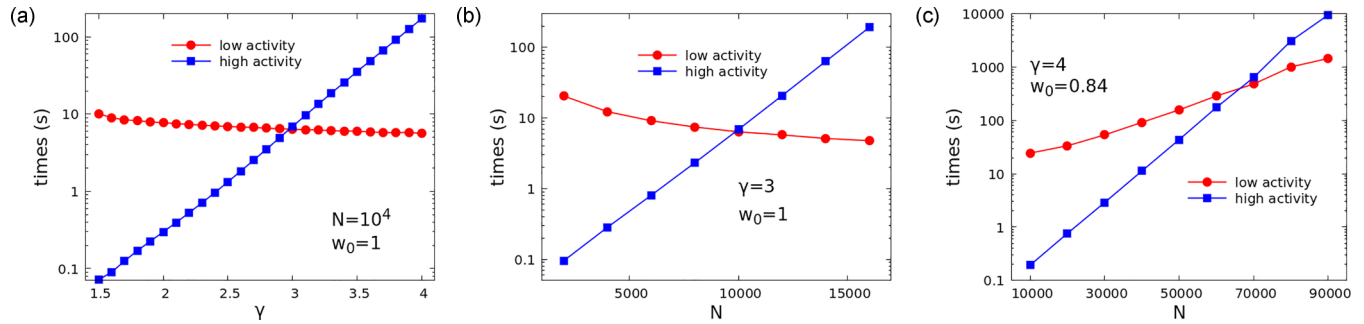

FIG. 7. (a) Lifetimes of low- and high-activity states for $N = 10^4$, $w_0 = 1$, as a function of γ. (b) Lifetimes of low- and high-activity states for $\gamma = 3$, $w_0 = 1$, as a function of the number of neurons. (c) The same for $\gamma = 4$, $w_0 = 0.84$.

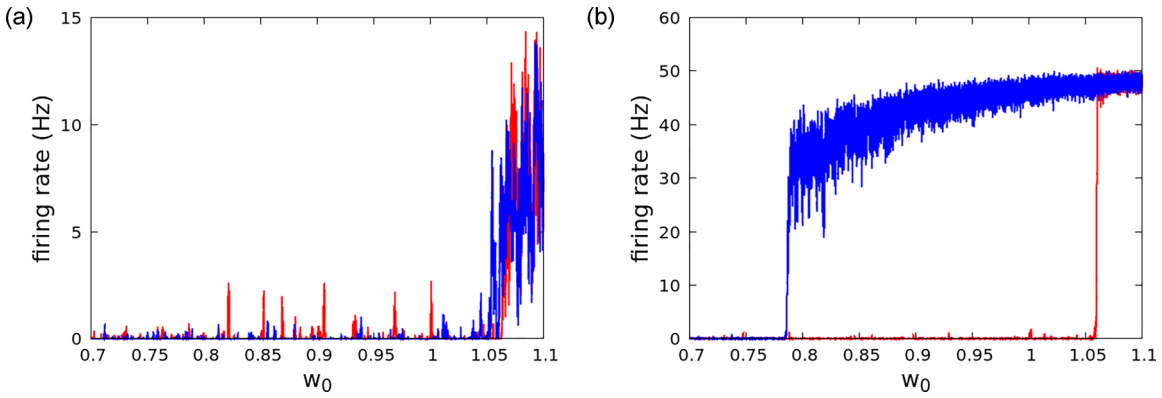

FIG. 8. Hysteresis loops for a system of $N = 10^5$ neurons, with (a) $\gamma = 0$ and (b) $\gamma = 4$. The parameter w_0 increases from $w_0 = 0.7$ to $w_0 = 1.1$ in 50 s, and then decreases back to the value $w_0 = 0.7$ in another 50 s. The lower red (upper blue) line shows the firing rate per neuron when w_0 is increased (decreased).

sizes and durations is an exponential and not a power law. We study the distribution of avalanches by the protocol commonly used in experiments; namely, we divide the time series of the activity of the network in time bins of width δ, and identify an avalanche as a continuous series of nonempty time bins. A time bin is empty if the number of spikes (neurons that pass from the inactive to the active state) is zero during the interval. The duration of the avalanche is defined as the number of contiguous time bins multiplied by the width δ, while the size of the avalanche is defined as the total number of spikes.

When the activity of the network is bistable, and the system switches from the low- to the high-activity state, we expect two different kinds of avalanches: the first are "normal" avalanches, given by bursts of activity that do not cross the threshold with the basin of attraction of the high-activity state, so that the system remains in the low-activity state; these should be distributed as a scale-free power law. The second kind of avalanche (large "anomalous" avalanche) occurs when the system crosses the threshold and falls in the high-activity state. In this latter case, we do not expect a scale-free distribution, but rather a Poissonian (exponential) tail of the durations (and sizes) with a very long characteristic time and size. The results are shown in Fig. 9, for a system with $N = 10^4$, $w_0 = 1$, and γ between 0 and 4. For $\gamma \geqslant 2$, where the system is bistable and the distribution of the activity is bimodal, one observes correspondingly a bimodal distribution of avalanches. The first part of the distributions, corresponding to the marginal "low-activity" state, can be well fitted by power laws, $P(S) \propto S^{-\alpha}$ and $P(T) \propto T^{-\beta}$, with exponents respectively $\alpha \simeq 1.47$ and $\beta \simeq 1.93$. Exponents were measured in the case $\gamma = 3$, with the POWERLAW package [35], considering sizes in the interval $50 < S < 5000$ and durations in the interval $5 < T < 300$ time bins.

In Fig. 9(b) we fit the long tail of the distribution with an exponential Poissonian distribution, to show that the long tail is indeed Poissonian. The characteristic times are between two and three times larger than those in Fig. 7(a), because when the system reaches the minimum in the bimodal distribution of the activity (and the high-activity state, as it is defined in Fig. 7, ends) it has a finite probability of returning back in the high-activity state without hitting the zero activity that ends the avalanche as we have defined it here.

In Fig. 9(c) we show the mean size $\langle S \rangle(T)$ of the avalanches having duration in a small interval around T. Also in this case we observe two characteristic regimes. In the first regime, corresponding to smaller avalanches characteristic of the scale-free low-activity state, the mean size scales as $\langle S \rangle(T) \sim T^k$, with $k = 2$, as expected from the relation $k = (\beta - 1)/(\alpha - 1)$, originally predicted in the theory of crackling noise [36,37]. In the second regime, corresponding to larger avalanches characteristic of the high-activity state, the exponent decreases to $k = 1$. Note that the same exponent characterizes large avalanches also for $\gamma \leqslant 1$, where only the low-activity fixed point of the dynamics exists, showing that it is a common feature of avalanches larger than the cutoff of the scale-free distribution, with an exponential distribution of durations, as already noted in Refs. [38,39]. The same behavior, with an exponent $k = 2$ for short avalanches and $k = 1$ for longer ones, was recently observed via electroencephalogram during sleep [40], in experiments on nonhuman primates [8] and in the cortex of awake mice [41]. In particular, in Ref. [41], a flattening of the shape of avalanches was observed for longer avalanches, also in this case in agreement with our results (see below).

In Fig. 9(d) we show the dependence of the distributions on the system size, that is, on the number of neurons, N. When N is small, we observe only the first regime of small avalanches, with a scaling of the cutoff of the power-law distribution with the system size. However, increasing N, avalanches tend to last longer than the lifetime of the low-activity state. At this point, very large avalanches switch with high probability to the high-activity state, so that one observes a saturation of the cutoff of the initial power-law distribution, and the appearance of the second exponential regime of large avalanches. In this case, increasing N just increases the lifetime of the high-activity state, and therefore the cutoff of the exponential distribution. Correspondingly, the number per unit time of large avalanches decreases, as evidenced by the lower values of the probability. Indeed, when N becomes very large, one expects to observe just a single very long avalanche during the observation time. However, as pointed out in the Introduction,

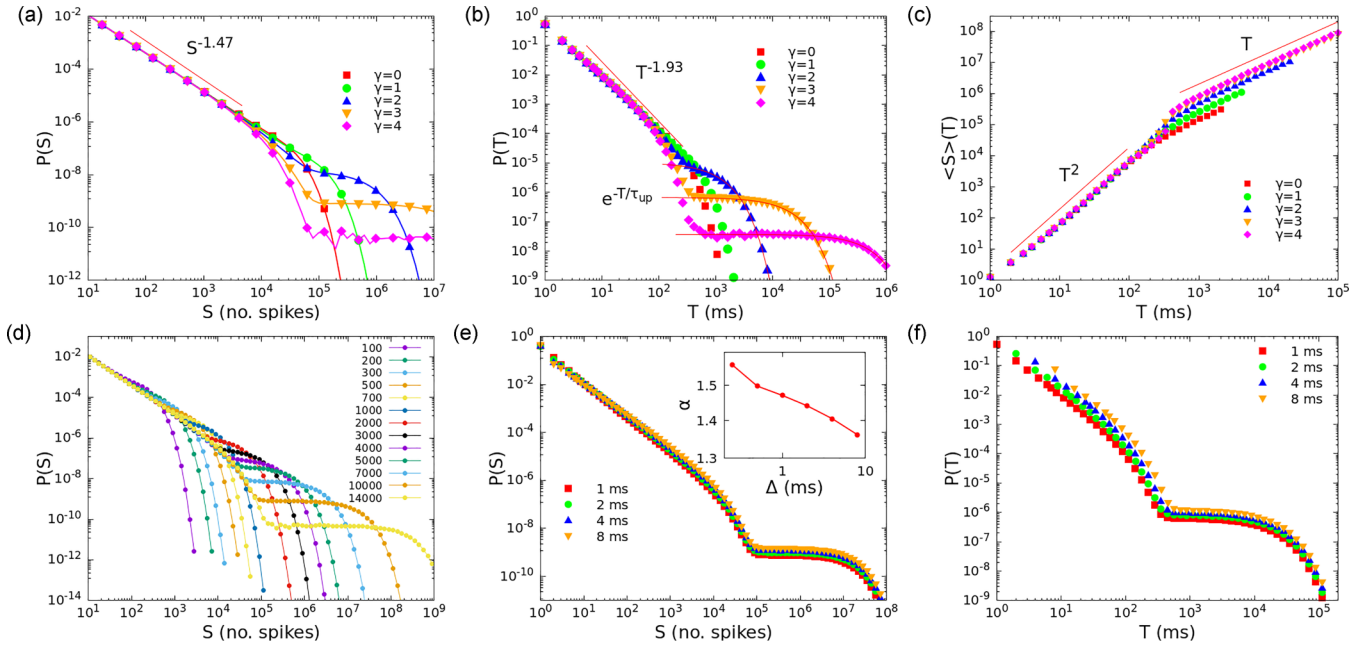

FIG. 9. Avalanche distributions, defined as histograms of the probability that an avalanche has a size or duration within some interval, divided by the width of the interval (logarithmic spacings). The parameters are taken on the second-order transition line and upper spinodal, $w_0 = 1$, with $N = 10^4$ and γ between 0 and 4. The width of the time bins is $\delta = 1$ ms. (a) Size distribution $P(S)$. The exponent was measured in the case $\gamma = 3$ for sizes $50 < S < 5000$. (b) Duration distribution $P(T)$. The exponent was measured in the case $\gamma = 3$ for durations $5 < T < 300$. (c) Mean size $\langle S \rangle (T)$ as a function of the duration of the avalanche. (d) Dependence of $P(S)$ on the number of neurons, for $w_0 = 1$, $\delta = 1$ ms, $\gamma = 3$, and $N = 100$ (leftmost) to $N = 14\,000$ (rightmost). (e) Dependence of $P(S)$ on the width of time bins δ, for $N = 10^4$, $w_0 = 1$, $\gamma = 3$. Inset: Power-law exponent α measured for avalanches with size $50 < S < 5000$. (f) Dependence of $P(T)$ on the width of time bins δ, for $N = 10^4$, $w_0 = 1$, $\gamma = 3$. Exponents were measured with the POWERLAW package [35].

a fully connected network as the one considered here is not intended to describe the behavior of very large regions of the brain.

Finally, in Figs. 9(e) and 9(f), we show the dependence of the distributions on the width δ of time bins. In this case, the overall normalization (increasing δ decreases the probability of small avalanches) is only slightly modified, but the value of the exponent of the first power-law regime is modified more substantially [inset of Fig. 9(e)].

Beside the low-activity state, one expects a critical behavior also for the high-activity state, near the lower spinodal of Fig. 3. However, the firing rate in the high-activity state fluctuates around a mean value, so to define avalanches it is necessary to define a threshold greater than zero, otherwise one would find very long Poissonian avalanches, as shown before. In Fig. 10 we show the result for $N = 10^4$, $\gamma = 2, 3, 4$. As already put in evidence in Ref. [25], avalanches defined with a finite threshold show critical exponents different from

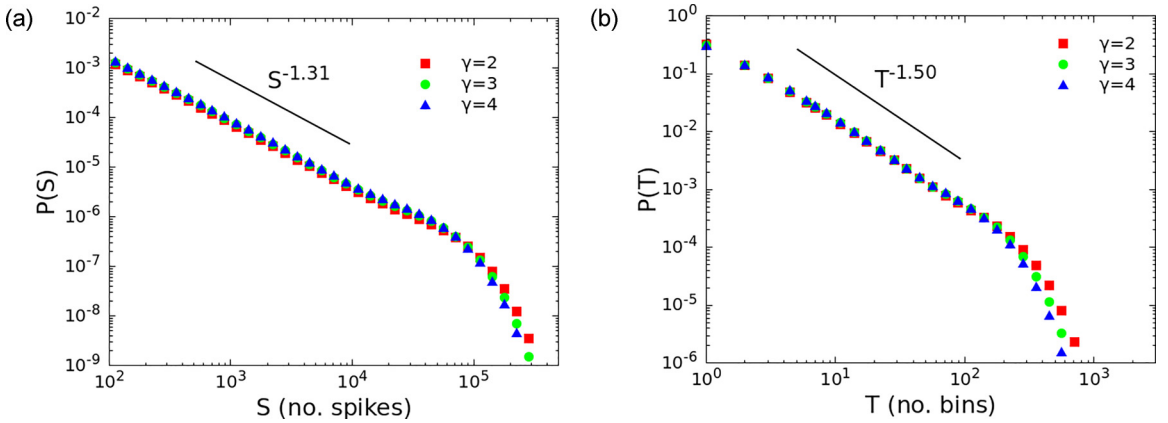

FIG. 10. Avalanche distributions on the lower spinodal, $w_0 = w(\gamma)$, defined with a finite threshold in the number of spikes in a time bin, $n_{\rm th} = N\delta R_0$, where R_0 is the firing rate per neuron at the high-activity fixed point. (a) Size distribution $P(S)$ for a system with $N = 10^4$, $\gamma = 2, 3, 4$, and the width of the time bins is $\delta = 1$ ms. The exponent was measured in the case $\gamma = 3$ for sizes $50 < S < 5000$. (b) Duration distribution $P(T)$. The exponent was measured in the case $\gamma = 3$ for durations $5 < T < 100$.

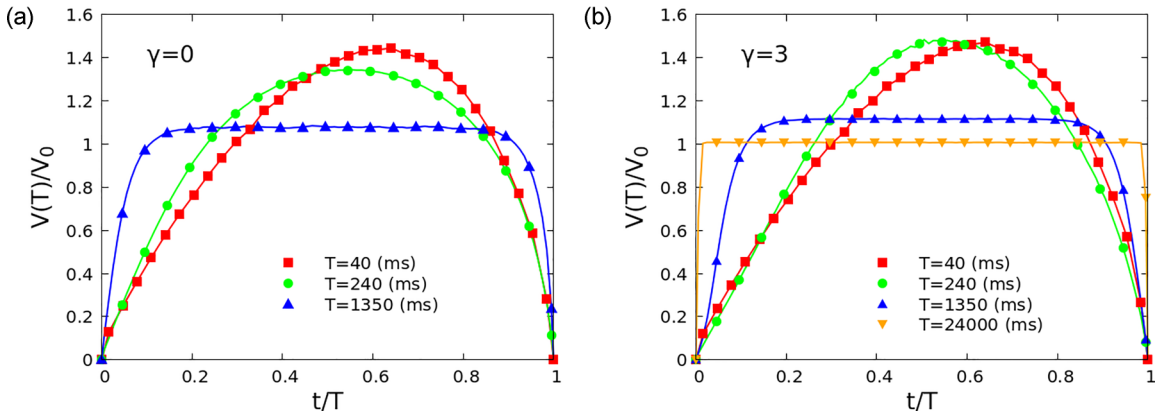

FIG. 11. Average normalized shape $V(t)/V_0$ of avalanches having durations in a small interval around T, for (a) $\gamma = 0$ and (b) $\gamma = 3$.

those of the branching model, and characteristic of the random walk.

Going back to avalanches defined in the low-activity state, in Fig. 11 we show the average normalized shape of avalanches as a function of their duration. The different nature of low-activity scale-free avalanches and high-activity Poissonian ones manifests itself also in the average shape. While avalanches of smaller duration have a quasiparabolic shape, those of longer duration tend to assume a flattened shape, more and more as the duration increases. As said before, this was recently observed also experimentally [41]. This is expected on quite general grounds, the effect depending on the different distribution of durations, that is a power law for short avalanches, and an exponential characterized by a cutoff for larger ones [38,39]. As observed for the exponent of $\langle S\rangle(T)$, also the shape of avalanches depends quite weakly on the parameter γ, and therefore on the existence of one or two fixed points of the dynamics, but mainly on their duration, that is, if they are shorter or longer than the cutoff of the power-law distribution.

A notable characteristic of the shape of avalanches in the critical regime is the rightward asymmetry. This feature depends on the "inertia" that characterizes the process: a positive inertia gives rise to a rightward asymmetry [38], while a negative one gives rise to a leftward asymmetry [42]. In the present model, the effective inertia is positive, because an imbalance with an excess of active excitatory or inhibitory neurons pushes the activity up or down (corresponding to positive or negative velocity, respectively) until the imbalance is reversed, so the rightward asymmetry is expected. In this respect, experimental results that show a leftward asymmetry [43] represent a question that needs further investigation.

IV. CONCLUSION

We have studied a stochastic version of the Wilson-Cowan model with the activation function (4) that combines two features. It is equal to zero when the input is lower than some threshold (here taken as zero) and is convex in some interval of the input above the threshold. In some region of the parameters w_0 and γ, the system therefore is characterized by two attractive fixed points, one of which corresponds to activity zero when the external input h goes to zero (which we call a "critical" or "low-activity" state) while the other corresponds to a finite activity when $h \to 0$, and therefore to a self-sustained activity of the network ("high-activity" persistent state). While for an infinite number of neurons the ratio of the lifetimes of the two states either goes to zero or diverges, so that only one of the states is selected, for a finite number of neurons the system switches between the two states, and displays a bistable activity. Moreover, as long as the lifetime of the states is much larger than the inverse rate of change of parameters, the system displays a hysteretic behavior.

The two different fixed points are characterized by very different behavior of the activity as a function of time. While in the high-activity state the activity fluctuates around a constant value corresponding to the fixed point, in the low-activity one it is characterized by bursts (avalanches) interspersed by periods of zero activity (quiescence). Defining avalanches as periods of time in which the activity is greater than zero, one therefore finds that their distribution is bimodal, with a first regime (small avalanches) corresponding to bursts of activity within the low-activity state, and a second regime (large avalanches) corresponding to periods of time in which the system remains in the high-activity state. On the so-called spinodal line, where the low-activity fixed point becomes unstable, the first part of the probability distribution becomes critical, with exponents characteristic of the mean field branching process, although with a cutoff that does not diverge with the system size, but rather saturates due to the finite lifetime of the low-activity state. This is due to the multiplicative coefficient of the noise in Eq. (1), which scales as the square root of the activity when the activity is near zero. On the other hand, the presence of the high-activity state is evidenced by a second regime (large avalanches) with a Poissonian (exponential) distribution. The two kinds of avalanches are characterized by a different scaling of the size as a function of the duration and shape. The size of critical avalanches scales as T^2, as expected in the branching process, and the shape is nearly parabolic, although slightly rightward asymmetric, as expected for a process characterized by a positive "inertia." Avalanches corresponding to the high-activity state instead are characterized by a size proportional to the duration, and a flattened shape, as expected for avalanches that have an exponential distribution of durations.

The bistable behavior of a stochastic version of the Wilson-Cowan model was already studied in Ref. [33], by considering an activation function with a superlinear behavior, namely, the sigmoidal function $f(s) = (1 + e^{-s})^{-1}$. In that paper the lifetimes of states were computed using a WKB approximation, but the distribution of avalanches of activity was not considered. Indeed, in that case both fixed points are characterized by a finite average activity, so that one could expect a critical behavior near spinodal lines, but with different exponents, characteristic of a random walk, as shown here in Fig. 10 for the avalanches at the lower spinodal. As pointed out in Ref. [25], the critical exponents of the branching model are expected only when the mean activity vanishes with the external input.

The model shows, in the critical state, exponents $\alpha \simeq 1.5$, $\beta \simeq 2$, $k \simeq 2$, characteristic of the mean field branching model. These exponents has been observed in different neural experimental results, including the original results in cortical slices [1]; however, there are also experimental results that have found deviations from these exponents [13,44], and different computational models [45–49] have tried to account for these deviations. In our model we find mean field branching model exponents, since the model is characterized by all-to-all connectivity. However, as shown in Ref. [49], the value of exponents changes when a different topology of the connections is considered, for example, short-range connections on a two-dimensional lattice. It should be possible to put together the spatial topology of the network with an activation function that gives rise to a bistable behavior, to produce a model that shows bistability and non-mean-field exponents.

In conclusion, this model could be relevant in the elucidation of the bistable behavior of neural networks in some conditions, like reduced inhibition, epileptic, or hyperexcitable conditions, where a bimodal distribution of avalanches is observed.

ACKNOWLEDGMENT

A.d.C. acknowledges financial support from the MIUR PRIN 2017WZFTZP "Stochastic forecasting in complex systems."

[1] J. M. Beggs and D. Plenz, Neuronal avalanches in neocortical circuits, J. Neurosci. **23**, 11167 (2003).
[2] T. Petermann, T. C. Thiagarajan, M. A. Lebedev, M. A. Nicolelis, D. R. Chialvo, and D. Plenz, Spontaneous cortical activity in awake monkeys composed of neuronal avalanches, Proc. Natl. Acad. Sci. USA **106**, 15921 (2009).
[3] O. Shriki, J. Alstott, F. Carver, T. Holroyd, R. N. Henson, M. L. Smith, R. Coppola, E. Bullmore, and D. Plenz, Neuronal avalanches in the resting MEG of the human brain, J. Neurosci. **33**, 7079 (2013).
[4] T. L. Ribeiro, M. Copelli, F. Caixeta, H. Belchior, D. R. Chialvo, M. A. L. Nicolelis, and S. Ribeiro, Spike avalanches exhibit universal dynamics across the sleep-wake cycle, PLoS One **5**, e14129 (2010).
[5] G. Hahn, T. Petermann, M. N. Havenith, S. Yu, W. Singer, D. Plenz, and D. Nikolic, Neuronal avalanches in spontaneous activity in vivo, J. Neurophysiol. **104**, 3312 (2010).
[6] T. Bellay, A. Klaus, S. Seshadri, and D. Plenz, Irregular spiking of pyramidal neurons organizes as scale-invariant neuronal avalanches in the awake state, Elife **4**, e07224 (2015).
[7] S. Yu, A. Klaus, H. Yang, and D. Plenz, Scale-invariant neuronal avalanche dynamics and the cut-off in size distributions, PLoS One **9**, e99761 (2014).
[8] S. R. Miller, S. Yu, and D. Plenz, The scale-invariant, temporal profile of neuronal avalanches in relation to cortical γ-oscillations, Sci. Rep. **9**, 16403 (2019).
[9] W. L. Shew, H. Yang, T. Petermann, R. Roy, and D. Plenz, Neuronal avalanches imply maximum dynamic range in cortical networks at criticality, J. Neurosci. **29**, 15595 (2009).
[10] V. Pasquale, P. Massobrio, L. L. Bologna, M. Chiappalone, and S. Martinoia, Self-organization and neuronal avalanches in networks of dissociated cortical neurons, Neuroscience **153**, 1354 (2008).
[11] H. Yang, W. L. Shew, R. Roy, and D. Plenz, Maximal variability of phase synchrony in cortical networks with neuronal avalanches, J. Neurosci. **32**, 1061 (2012).
[12] M. Yaghoubi, T. de Graaf, J. G. Orlandi, F. Girotto, M. A. Colicos, and J. Davidsen, Neuronal avalanche dynamics indicates different universality classes in neuronal cultures, Sci. Rep. **8**, 3417 (2018).
[13] N. Friedman, S. Ito, B. A. W. Brinkman, M. Shimono, R. E. Lee DeVille, K. A. Dahmen, J. M. Beggs, and T. C. Butler, Universal Critical Dynamics in High Resolution Neuronal Avalanche Data, Phys. Rev. Lett. **108**, 208102 (2012).
[14] L. Cocchi, L. L. Gollo, A. Zalesky, and M. Breakspear, Criticality in the brain: A synthesis of neurobiology, models and cognition, Prog. Neurobio. **158**, 132 (2017).
[15] J. O'Byrne and K. Jerbi, How critical is brain criticality? Trends Neurosci. **45**, 820 (2022).
[16] D. Plenz, T. L. Ribeiro, S. R. Miller, P. A. Kells, A. Vakili, and E. L. Capek, Self-organized criticality in the brain, Front. Phys. **9**, 639389 (2021).
[17] D. R. Chialvo, Emergent complex neural dynamics, Nat. Phys. **6**, 744 (2010).
[18] O. Kinouchi and M. Copelli, Optimal dynamical range of excitable networks at criticality, Nat. Phys. **2**, 348 (2006).
[19] W. L. Shew, H. Yang, S. Yu, R. Roy, and D. Plenz, Information capacity and transmission are maximized in balanced cortical networks with neuronal avalanches, J. Neurosci. **31**, 55 (2011).
[20] L. de Arcangelis, C. Perrone-Capano, and H. J. Herrmann, Self-Organized Criticality Model for Brain Plasticity, Phys. Rev. Lett. **96**, 028107 (2006).
[21] A. Levina, J. M. Herrmann, and T. Geisel, Dynamical synapses causing self-organized criticality in neural networks, Nat. Phys. **3**, 857 (2007).
[22] D. Millman, S. Mihalas, A. Kirkwood, and E. Niebur, Self-organized criticality occurs in non-conservative neuronal networks during 'up' states, Nat. Phys. **6**, 801 (2010).
[23] S. Scarpetta and A. de Candia, Neural avalanches at the critical point between replay and non-replay of spatiotemporal patterns, PLoS One **8**, e64162 (2013).

[24] M. Benayoun, J. D. Cowan, W. van Drongelen, and E. Wallace, Avalanches in a stochastic model of spiking neurons, PLoS Comput. Biol. **6**, e1000846 (2010).

[25] A. de Candia, A. Sarracino, I. Apicella, and L. de Arcangelis, Critical behaviour of the stochastic Wilson-Cowan model, PLoS Comput. Biol. **17**, e1008884 (2021).

[26] E. D. Gireesh and D. Plenz, Neuronal avalanches organize as nested theta- and beta/gamma-oscillations during development of cortical layer 2/3, Proc. Natl. Acad. Sci. USA **105**, 7576 (2008).

[27] L. de Arcangelis, Are dragon-king neuronal avalanches dungeons for self-organized brain activity? Eur. Phys. J. Spec. Top. **205**, 243 (2012).

[28] D. Sornette and G. Ouillon, Dragon-kings: Mechanisms, statistical methods and empirical evidence, Eur. Phys. J. Spec. Top. **205**, 1 (2012).

[29] S. H. Wang, G. Arnulfo, V. Myrov, F. Siebenhühner, L. Nobili, M. Breakspear, S. Palva, and J. M. Palva, Critical-like bistable dynamics in the resting-state human brain, https://www.biorxiv.org/content/10.1101/2022.01.09.475554v1.

[30] A. Tran-Van-Minh, R. D. Cazé, T. Abrahamsson, L. Cathala, B. S. Gutkin, and D. A. DiGregorio, Contribution of sublinear and supralinear dendritic integration to neuronal computations, Front. Cell. Neurosci. **9**, 67 (2015).

[31] A. Sarracino, O. Arviv, O. Shriki, and L. de Arcangelis, Predicting brain evoked response to external stimuli from temporal correlations of spontaneous activity, Phys. Rev. Res. **2**, 033355 (2020).

[32] N. G. van Kampen, *Stochastic Processes in Physics and Chemistry* (North-Holland, Amsterdam, 2007).

[33] P. C. Bressloff, Metastable states and quasicycles in a stochastic Wilson-Cowan model of neuronal population dynamics, Phys. Rev. E **82**, 051903 (2010).

[34] D. Gillespie, Exact stochastic simulation of coupled chemical reactions, J. Phys. Chem. **81**, 2340 (1977).

[35] J. Alstott, E. Bullmore, and D. Plenz, POWERLAW: A PYTHON package for analysis of heavy-tailed distributions, PLoS One **9**, e85777 (2014).

[36] M. C. Kuntz and J. P. Sethna, Noise in disordered systems: The power spectrum and dynamic exponents in avalanche models, Phys. Rev. B **62**, 11699 (2000).

[37] J. P. Sethna, K. A. Dahmen, and C. R. Myers, Crackling noise, Nature (London) **410**, 242 (2001).

[38] A. Baldassarri, F. Colaiori, and C. Castellano, Average Shape of a Fluctuation: Universality in Excursions of Stochastic Processes, Phys. Rev. Lett. **90**, 060601 (2003).

[39] S. Papanikolaou, F. Bohn, R. L. Sommer, G. Durin, S. Zapperi, and J. P. Sethna, Universality beyond power laws and the average avalanche shape, Nat. Phys. **7**, 316 (2011).

[40] S. Scarpetta, N. Morrisi, C. Mutti, N. Azzi, I. Trippi, R. Ciliento, I. Apicella, G. Messuti, M. Angiolelli, F. Lombardi, L. Parrino, and A. E. Vaudano, Criticality of neuronal avalanches in human sleep and their relationship with sleep macro- and micro-architecture, https://www.biorxiv.org/content/10.1101/2022.07.12.499725v2.

[41] E. Capek, T. L. Ribeiro, P. Kells, K. Srinivasan, S. R. Miller, E. Geist, M. Victor, A. Vakili, S. Pajevic, D. R. Chialvo, and D. Plenz, Parabolic avalanche scaling in the synchronization of cortical cell assemblies, https://www.biorxiv.org/content/10.1101/2022.11.02.514938v1.

[42] S. Zapperi, C. Castellano, F. Colaiori, and G. Durin, Signature of effective mass in crackling-noise asymmetry, Nat. Phys. **1**, 46 (2005).

[43] J. A. Roberts, K. K. Iyer, S. Finnigan, S. Vanhatalo, and M. Breakspear, Scale-free bursting in human cortex following hypoxia at birth, J. Neurosci. **34**, 6557 (2014).

[44] A. J. Fontenele, N. A. P. de Vasconcelos, T. Feliciano, L. A. A. Aguiar, C. Soares-Cunha, B. Coimbra, L. Dalla Porta, S. Ribeiro, A. J. Rodrigues, N. Sousa, P. V. Carelli, and M. Copelli, Criticality between Cortical States, Phys. Rev. Lett. **122**, 208101 (2019).

[45] D. J. Korchinski, J. G. Orlandi, S. W. Son, and J. Davidsen, Criticality in Spreading Processes without Timescale Separation and the Critical Brain Hypothesis, Phys. Rev. X **11**, 021059 (2021).

[46] R. V. Williams-García, J. M. Beggs, and G. Ortiz, Unveiling causal activity of complex networks, Europhys. Lett. **119**, 18003 (2017).

[47] T. T. A. Carvalho, A. J. Fontenele, M. Girardi-Schappo, T. Feliciano, L. A. A. Aguiar, T. P. L. Silva, N. A. P. de Vasconcelos, P. V. Carelli, and M. Copelli, Subsampled directed-percolation models explain scaling relations experimentally observed in the brain, Front. Neural Circuits **14**, 576727 (2021).

[48] L. D. Porta and M. Copelli, Modeling neuronal avalanches and long-range temporal correlations at the emergence of collective oscillations: Continuously varying exponents mimic M/EEG results, PLoS Comput. Biol. **15**, e1006924 (2019).

[49] I. Apicella, S. Scarpetta, L. de Arcangelis, A. Sarracino, and A. de Candia, Power spectrum and critical exponents in the 2D stochastic Wilson Cowan model, Sci. Rep. **12**, 21870 (2022).